

Experimental study on the vibrational relaxation mechanism of $N_2(X^1\Sigma_g^+, v = 6)$ molecules in collision with N_2, O_2, and CO

Yaqi Zhang(张亚琦), Yuhao Wu(武宇豪), Jing Liu(刘静), Jiaxin Lin(林佳欣), and Maofu Yu(于茂福)
Citation: Chin. Phys. B, 2026, 35 (**3**): 033401. DOI: 10.1088/1674-1056/adf82e
http://cpb.iphy.ac.cn; http://iopscience.iop.org/cpb

What follows is a list of articles you may be interested in

Single electron capture in low- and intermediate-energy collisions of $Si^{3,4+}$ with He

Yingzhou Li(李英卓), Yadong Liu(刘亚东), Yueying Qi(祁月盈), Ling Liu(刘玲), Yizhi Qu(屈一至), and Jianguo Wang(王建国)
Chin. Phys. B, 2026, 35 (**1**): 013401. DOI: 10.1088/1674-1056/ae15f4

Experiment study of energy redistribution during collisions of the excited state $H_2(1, 7)$ with LiH

Kai Wang(王凯), Zhong Liu(刘中), Shuying Wang(王淑英), Chu Qin(秦楚), Zilei Yu(於子雷), and Xiaofang Zhao(赵小芳)
Chin. Phys. B, 2025, 34 (**11**): 113401. DOI: 10.1088/1674-1056/add502

Electron excitation processes in low energy collisions of hydrogen-helium atoms

Kun Wang(王堃), Chuan Dong(董川), Yi-Zhi Qu(屈一至), Ling Liu(刘玲), Yong Wu(吴勇),Xu-Hai Hong(洪许海), and Robert J. Buenker
Chin. Phys. B, 2022, 31 (**12**): 123401. DOI: 10.1088/1674-1056/aca14c

Li(2p $\leftarrow$ 2s) + Na(3s) pressure broadening in the far-wing and line-core profiles

F Talbi, N Lamoudi, L Reggami, M T Bouazza, K Alioua, and M Bouledroua
Chin. Phys. B, 2022, 31 (**7**): 073401. DOI: 10.1088/1674-1056/ac43a0

Charge transfer in low-energy collisions ofBe^{3+} and B^{4+} ions with He

Kun Wang(王堃), Yi-Zhi Qu(屈一至), Chun-Hua Liu(刘春华), Ling Liu(刘玲), Yong Wu(吴勇), H P Liebermann, Robert J. Buenker
Chin. Phys. B, 2020, 29 (**9**): 093401. DOI: 10.1088/1674-1056/aba276

Experimental study on the vibrational relaxation mechanism of $N_2(X^1\Sigma_g^+, v = 6)$ molecules in collision with N_2, O_2, and CO

Yaqi Zhang(张亚琦)[1,2,†], Yuhao Wu(武宇豪)[1,2,†], Jing Liu(刘静)[1,2,‡], Jiaxin Lin(林佳欣)[1,2], and Maofu Yu(于茂福)[1,2]

[1] *Xinjiang Key Laboratory of Solid State Physics and Devices, Xinjiang University, Urumqi* 830017, *China*
[2] *School of Physical Science and Technology, Xinjiang University, Urumqi* 830017, *China*

(Received 2 July 2025; revised manuscript received 1 August 2025; accepted manuscript online 6 August 2025)

This study employed time-resolved coherent anti-Stokes Raman scattering to investigate the vibrational relaxation mechanism of N_2 ($v = 6$) molecules in N_2–M systems, where M denotes N_2, O_2, or CO. At 297 K, the relaxation rate coefficients for collisions between N_2 ($v = 6$) and N_2, O_2, and CO were determined to be $(2.85 \pm 0.07) \times 10^{-14}$ cm^3·s^{-1}, $(6.29 \pm 0.12) \times 10^{-14}$ cm^3·s^{-1}, and $(11.21 \pm 0.20) \times 10^{-14}$ cm^3·s^{-1}, respectively. The results demonstrated that the relaxation rate coefficient for N_2 ($v = 6$)–CO collisions was 1.8 times higher than that for N_2–O_2 collisions and 3.9 times greater than that for homonuclear N_2–N_2 collisions, indicating that CO significantly enhances the vibrational relaxation of N_2 ($v = 6$). Furthermore, by analyzing the time-resolved population evolution of N_2 ($v \leq 6$) in N_2–O_2 and N_2–CO systems under varying buffer gas molar ratios and integrating these data with kinetic analysis, the vibrational relaxation mechanism of N_2 ($v = 6$) in different collisional environments was systematically elucidated. The findings indicate that in the N_2–O_2 system, increasing the molar ratio of acceptor molecules leads to a gradual shift from single-quantum to multi-quantum relaxation dominance, whereas the N_2–CO system exhibits a transition from multi-quantum to single-quantum dominance. In addition, a systematic study examined the vibrational relaxation mechanism of N_2 ($v = 6$) in two gas mixtures between 297 K and 573 K. The results indicate that elevated temperature significantly enhances the efficiency of near-resonance energy transfer associated with the dominant relaxation pathway.

Keywords: collision relaxation rate coefficients, vibrational energy near-resonance quantum exchange, multi-quantum relaxation mechanism, temperature dependence

PACS: 34.50.Ez, 34.20.–b, 33.80.–b, 42.65.Dr

DOI: 10.1088/1674-1056/adf82e **CSTR:** 32038.14.CPB.adf82e

1. Introduction

The energy transfer and redistribution mechanisms involved in intermolecular collision processes are an important area of research in molecular dynamics and chemical physics.[1–4] In complex gaseous environments, such as those encountered in astrochemistry, combustion processes, plasma physics, and hypersonic aerodynamics,[5–9] which involve non-local thermodynamic equilibrium conditions, the population distribution of molecular energy levels often deviates from the Boltzmann distribution. In these systems, molecules gain or lose vibrational and rotational energy through various collision processes; the redistribution among internal energy modes significantly affects the microscopic dynamics of non-equilibrium processes. Specifically, inelastic transition processes induced by molecular collisions (including vibration–translation/rotation (V–T/R), vibration–rotation (V–R), vibration–vibration (V–V), as well as rotation–rotation (R–R) and rotation–vibration (R–V) energy exchange mechanisms) are key factors that drive gas systems towards thermal equilibrium. Among these processes, the state-to-state collision relaxation rate coefficients play a decisive role, directly influencing the prediction accuracy of non-equilibrium state models.

N_2 is the dominant constituent of Earth's atmosphere and a key component of the atmospheres of several celestial bodies, including Titan, Enceladus, Pluto, Mars, and regions of the interstellar medium.[10–13] The study of N_2 molecular collision-induced energy transfer processes is of significant importance in the fields of chemical reaction dynamics and astrophysics, such as interstellar exploration, planetary entry dynamics, and high-altitude atmospheric processes.[14–22] In recent years, extensive theoretical research has been conducted on the ground-state electronic energy structure of N_2 molecules and their collision-induced energy transfer mechanisms involving gas-phase interactions. Current theoretical studies mainly employ either theoretical models (such as the forced harmonic-oscillator theory[17,19]) or computationally efficient dynamical methods to generate state-to-state collision relaxation rate coefficient datasets, including quasi-classical trajectory (QCT) methods and mixed quantum-classical methods (MQC).[23–29] Hong *et al.*[25,26] used the MQC dynamical method to calculate the V–V and V–T/R relaxation rate coefficients for CO–N_2 molecular collisions and systematically

[†] These authors contributed equally to this work.
[‡] Corresponding author. E-mail: xdlj@xju.edu.cn

© 2026 Chinese Physical Society and IOP Publishing Ltd. All rights, including for text and data mining, AI training, and similar technologies, are reserved.

computed a complete dataset of V–V and V–T/R relaxation rate coefficients for N_2–N_2 collisions. The results showed good consistency with existing experimental data for low vibrational energy levels. In a recent study, Yang *et al.*[27] applied this method to the N_2–O_2 system, obtaining rate coefficients for V–V and V–T/R energy exchange in O_2–N_2 collisions over a wide temperature range. The computed vibrational relaxation rate coefficients were in agreement with experimental data for low vibrational states. However, results from theoretical models do not always align with experimental data. Andrienko *et al.*[28] used the QCT method to calculate the V–V and V–T/R relaxation rate coefficients for O_2–N_2 collisions involving low vibrational states, and their results showed discrepancies with experimental data at low temperatures. Garcia *et al.*[29] investigated energy exchange processes in non-reactive O_2–N_2 collisions using the MQC method, with results indicating significant discrepancies between theoretical calculations and experimental data. Therefore, further refinement of theoretical models requires additional high-precision experimental data for validation.

Compared to theoretical studies, experimental data on the non-reactive collision energy transfer processes of N_2 molecules remain relatively limited.[30–36] Martínez *et al.*[34] measured the V–V collision rate coefficients between the $v = 1$ and $v = 0$ states of N_2 molecules in the temperature range of 77–300 K using time-resolved dual-resonance pump–probe techniques. The results indicated a strong negative temperature dependence of the rate coefficients within this temperature range. Xiao *et al.*[35] employed stimulated Raman pumping to excite N_2 ($v = 2$) molecules and combined it with resonance-enhanced multi-photon ionization techniques to reveal the physical mechanisms behind low cross-section excitation. Sitz and Farrow[36] measured the energy transfer rates between different rotational states of N_2 ($v = 1$) molecules at 298 K. These experimental studies have primarily focused on low vibrational excited states of N_2 molecules, while the experimental investigation of collision relaxation processes and energy transfer mechanisms in highly vibrationally excited N_2 states still requires further exploration. Conducting experimental studies on the collision relaxation processes of highly vibrationally excited N_2 molecules not only helps to reveal microscopic dynamical laws, such as molecular vibrational excitation and electronic transitions, but also provides more accurate data to support the development of theoretical models for energy transfer pathways in molecular vibration modes.

This study utilizes degenerate stimulated hyper-Raman pumping (DSHRP) to selectively populate N_2 molecules in the $v = 6$ vibrational level of the ground electronic state. By measuring the time-resolved CARS signals of N_2 ($v = 6$) molecules in the N_2–M ($M = N_2$, O_2, CO) system, and combining with the Stern–Volmer equation, the collision relaxation rate coefficients between N_2 and M molecules were obtained. At 297 K, the evolution of the population distribution of N_2 ($v = 5$, 4) molecules with respect to the delay time was measured in the N_2–O_2 and N_2–CO gas mixture systems. The relaxation mechanisms of N_2 ($v = 6$) molecules in different buffer gas environments were analyzed and discussed, and the effect of temperature on collision energy transfer mechanisms in N_2–O_2 and N_2–CO systems was systematically studied.

2. Experimental setup

A schematic diagram of the experimental setup is shown in Fig. 1. The sample cell used in the experiment is a custom-made stainless steel six-way cross tube with four horizontally aligned ports, each equipped with high-transmission optical windows. The top of the sample cell is connected to a four-way valve, which is further connected to the vacuum system, gas cylinders, and a vacuum gauge. A needle valve is installed at the gas inlet to regulate the gas flow. The external surface of the sample cell is wrapped with a flexible heating jacket to ensure uniform temperature distribution, with the temperature monitored in real time by a thermocouple. During the experiment, the entire sample cell was first evacuated to a pressure of 10^{-4} Pa using the vacuum system, after which the valve connected to the vacuum system was closed. The sample cell was purged with high-purity N_2 or gas mixtures (N_2–O_2 or N_2–CO), with the gas flow regulated by a needle valve. For pure N_2, the pressure was varied between 200 Torr and 600 Torr. For mixtures, the total pressure was fixed at 400 Torr, while the molar ratio of O_2 or CO was adjusted to 0.3–0.8. The N_2, O_2, and CO gases used in the experiment were of high purity (99.999%).

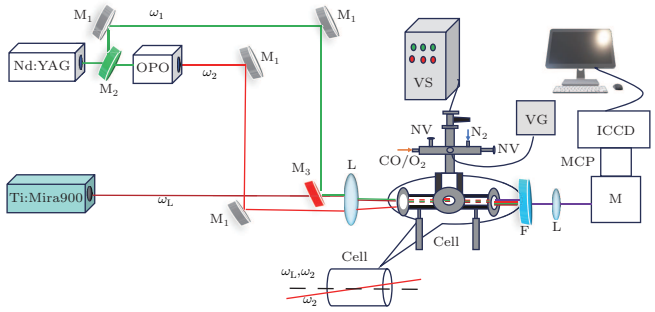


Fig. 1. Schematic of the experimental setup. OPO: optical parametric oscillator; M_1: full-band reflector; M_2: partial reflector; M_3: dichroic mirror; L: lens; F: filter; VS: vacuum system; VG: vacuum gauge; NV: needle valve; M: monochromator; MCP: microchannel plate; ICCD: intensified charge-coupled device.

Using a 738 nm laser output from a Ti:sapphire laser (Mira900), N_2 molecules are selectively excited to the $v = 6$ vibrational level of the ground electronic state via degenerate stimulated hyper-raman pumping. Subsequently, N_2 ($v = 6$) molecules undergo collisional transitions to lower vibrational levels through interactions with N_2, O_2, or CO molecules.

The population distribution of N_2 molecules across different vibrational states is probed using CARS spectroscopy. The pump light (ω_1) is provided by a 532 nm laser output from a frequency-doubled Nd:YAG laser (Brilliant MNL205-C), while the probe light (ω_2) originates from an optical parametric oscillator (OPO, Raind/Nir-D/S). After modulation by optical components, such as mirrors and a dichroic mirror, the two laser beams intersect at a small angle and enter the sample cell. A set of optical filters is positioned behind the sample cell to block scattered light and laser interference, ensuring the purity of the signal. The CARS signal ($\omega_{\mathrm{CARS}} = 2\omega_1 - \omega_2$) is focused by a convex lens and coupled into an optical fiber probe. The signal is then dispersed by a monochromator, amplified by a microchannel plate (MCP), and recorded by an intensified charge-coupled device (ICCD; sr-500i-bi). Notably, both the monochromator and MCP modules are integrated into the ICCD unit.

The principles of DSHRP excitation and CARS detection are shown in Fig. 2. ω_{L} is the frequency of the DSHRP pump light, and ω_1 and ω_2 are the frequencies of the pump and probe lights for CARS detection, respectively.

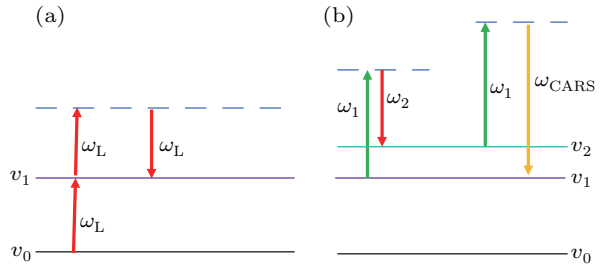


Fig. 2. Pump–probe schematic of N_2 molecules. (a) DSHRP excitation process; (b) CARS detection process.

3. Results and discussion

3.1. Determination of relaxation rate coefficients

Pure N_2, N_2–O_2 gas mixtures, or N_2–CO gas mixtures were introduced into the sample cell, with the temperature maintained at 297 K. Vibrationally excited N_2 ($v = 6$) molecules were generated using degenerate stimulated hyper-raman pumping. The effective lifetime and de-excitation rates of N_2 ($v = 6$) were determined by measuring the time-resolved CARS signals from the N_2 ($v = 6$) energy level under various conditions.

The particle number density at the excited N_2 ($v = 6$) level can be approximated as

$$N_v(t) = N_0 \mathrm{e}^{\frac{-t_{\mathrm{D}}}{\tau}}. \tag{1}$$

Here, $N_v(t)$ denotes the particle number density at the vibrational energy level of N_2 molecules, N_0 represents the initial population density at the vibrational state, and t_{D} is the delay time. τ refers to the effective lifetime of the excited N_2 ($v = 6$) molecules.

The relationship between the CARS signal and the population density is described by[37]

$$I_v \propto (N_v - N_{v+n})^2 I_{\mathrm{pump}}^2 I_{\mathrm{probe}}. \tag{2}$$

Here, I_v represents the relative intensity of the CARS signal, while I_{pump} and I_{probe} are the intensities of the pump and probe light, respectively. In this experiment, N_2 molecules are excited to the $v = 6$ vibrational state, and the population of the upper energy levels corresponding to the detected CARS signal is approximated as zero. By substituting Eq. (1) into Eq. (2), the relationship between the semi-logarithmic CARS signal and the effective lifetime of N_2 ($v = 6$) molecules can be derived as

$$\frac{1}{2}\ln\left(\frac{I_v(t_{\mathrm{D}})}{I_0}\right) = -\frac{t_{\mathrm{D}}}{\tau}. \tag{3}$$

Here, I_0 represents the initial CARS signal intensity.

3.1.1. Collision self-relaxation rate coefficients of N_2 ($v = 6$) molecules in the pure N_2 system

Pure N_2 was introduced into the sample cell at pressures ranging from 200 Torr to 600 Torr, with the temperature maintained at 297 K using a flexible heating jacket. N_2 molecules were excited to the $v = 6$ vibrationally excited state of the ground electronic state via degenerate stimulated hyper-raman pumping. Subsequently, time-resolved CARS signals of N_2 ($v = 6$) molecules were measured under different pressures. Figure 3 presents the semi-logarithmic fits of the time-resolved CARS signals at various pressures. The slope of the fitted line yields the de-excitation rates and effective lifetimes of N_2 ($v = 6$) molecules under different pressures, with the results summarized in Table 1.

Table 1. Effective lifetimes and de-excitation rates of N_2 ($v = 6$) energy levels at different pressures.

P (Torr)	200	300	400	500	600
Lifetime (μs)	5.24 ± 0.31	3.66 ± 0.19	2.72 ± 0.09	2.19 ± 0.06	1.78 ± 0.04
$1/\tau$ (10^5 s^{-1})	1.91 ± 0.12	2.73 ± 0.15	3.67 ± 0.13	4.56 ± 0.13	5.63 ± 0.12

The self-relaxation rate coefficient of the excited-state molecules in a single gas system is obtained using the Stern–Volmer equation[38]

$$\frac{1}{\tau} = \frac{1}{\tau_0} + k_v N. \tag{4}$$

Here, τ is the effective lifetime of the excited-state molecules, τ_0 is the spontaneous emission lifetime of the molecules, k_v is the collision self-relaxation rate coefficient, and N is the particle number density. Since the spontaneous emission of vibrationally excited N_2 molecules is minimal, $1/\tau_0$ is approximated as zero. At 297 K, the Stern–Volmer plot for the pure N_2 system is shown in Fig. 4.

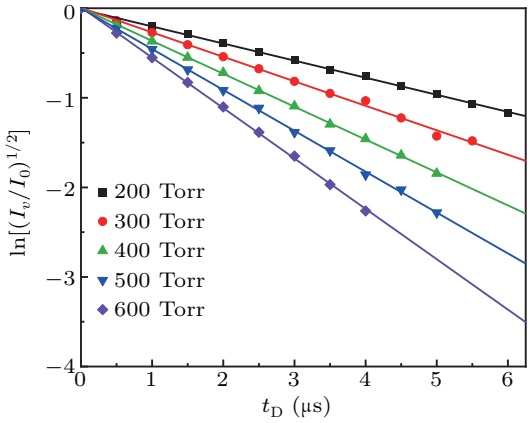


Fig. 3. Semi-logarithmic fits of time-resolved CARS intensity for N_2 ($v = 6$) molecules at different pressures.

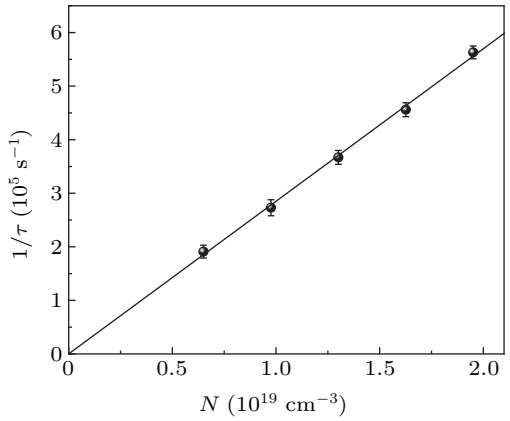


Fig. 4. Stern–Volmer plot for the pure N_2 system at 297 K.

The slope of the fitted line gives the self-relaxation rate coefficient for N_2 ($v = 6$) molecule collisions in the pure N_2 system, $k_v(N_2) = (2.85 \pm 0.07) \times 10^{-14}$ cm^3·s^{-1}. Billing and Fisher[39] computed the V–V collision energy transfer rate coefficients between excited-state N_2 ($v = 1$–19) and N_2 ($v = 1$) at 300 K using a semi-classical collision model, obtaining values on the order of 10^{-14} cm^3·s^{-1}. Hong *et al.*[26] using an improved MQC method, derived a comprehensive dataset for the V–V collision relaxation rate coefficients between N_2–N_2 at 300 K, ranging from 10^{-18} cm^3·s^{-1} to 10^{-14} cm^3·s^{-1}, which is in good agreement with the findings of the present study.

3.1.2. Collision relaxation rate coefficients of N_2 ($v = 6$) molecules in the N_2–O_2/CO system

At a sample cell temperature of 297 K, N_2–O_2/CO gas mixtures with a total pressure of 400 Torr and an O_2/CO molar ratio ranging from 0.3 to 0.8 were introduced. N_2 molecules were excited to the $v = 6$ vibrational state of the ground electronic state, and time-resolved CARS spectra of the N_2 ($v = 6$) energy level were measured under different molar ratios of the gas mixtures. Figure 5 shows the semi-logarithmic fits of the time-resolved CARS signals of N_2 ($v = 6$) molecules at various buffer gas molar ratios in the N_2–O_2 and N_2–CO gas mixtures. The effective lifetimes and de-excitation rates of the N_2 ($v = 6$) energy level in the N_2–O_2 and N_2–CO systems at different O_2/CO ratios are listed in Table 2. Here, τ_1 and τ_2 represent the effective lifetimes of the N_2 ($v = 6$) energy level in the N_2–O_2 and N_2–CO systems, respectively.

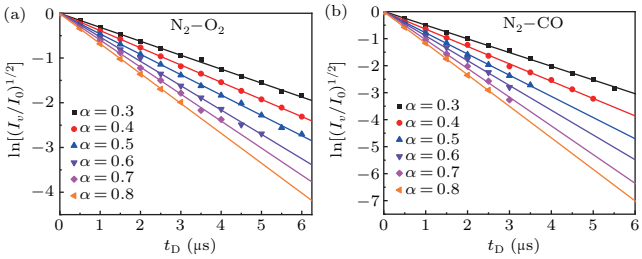


Fig. 5. Semi-logarithmic fits of the time-resolved CARS signals of N_2 ($v = 6$) molecules at different molar ratios: (a) N_2–O_2 system; (b) N_2–CO system.

Table 2. Effective lifetimes and de-excitation rates of N_2 ($v = 6$) energy levels in the gas mixtures system.

α	0.3	0.4	0.5	0.6	0.7	0.8
τ_1 (μs)	3.21 ± 0.12	2.60 ± 0.07	2.20 ± 0.04	1.84 ± 0.04	1.65 ± 0.02	1.49 ± 0.02
$1/\tau_1$ (10^5 s^{-1})	3.11 ± 0.13	3.84 ± 0.12	4.54 ± 0.09	5.43 ± 0.15	6.03 ± 0.09	6.67 ± 0.12
τ_2 (μs)	1.97 ± 0.05	1.56 ± 0.03	1.28 ± 0.02	1.09 ± 0.02	0.94 ± 0.01	0.86 ± 0.01
$1/\tau_2$ (10^5 s^{-1})	5.08 ± 0.15	6.42 ± 0.14	7.84 ± 0.15	9.17 ± 0.16	10.63 ± 0.13	11.68 ± 0.19

The collision relaxation rate coefficient of N_2 ($v = 6$) molecules can be obtained from the Stern–Volmer equation for the gas mixture system

$$\frac{1}{\tau} = \frac{1}{\tau_0} + \frac{P}{k_B T}\left[k_v(N_2)(1-\alpha) + \alpha k_v(M)\right]. \quad (5)$$

Here, τ represents the effective lifetime of the excited-state molecules, and α is the molar ratio of the buffer gas molecules in the gas mixture system. P is the total pressure of the system, k_B is the Boltzmann constant, and T is the temperature of the gas system. M denotes the buffer molecules (O_2 or CO) involved in the collision. $k_v(N_2)$ is the self-relaxation rate coefficient for N_2 ($v = 6$) molecules, and $k_v(M)$ is the collision relaxation rate coefficient for N_2 ($v = 6$) molecules with M molecules.

The particle number density in the gas mixture system is given by $N = P/(k_B T)$. Substituting this into Eq. (5) yields

$$\frac{1}{N\tau} = \alpha\left(k_v(M) - k_v(N_2)\right) + k_v(N_2). \quad (6)$$

Substituting the data listed in Table 2 into Eq. (6) gives the Stern–Volmer plot for N_2 ($v = 6$) molecules in the N_2–O_2 and

N_2–CO mixed systems, as shown in Fig. 6.

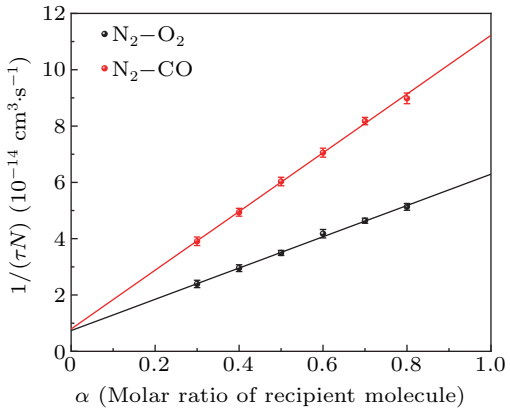


Fig. 6. Stern–Volmer plot for the gas mixtures system at 297 K.

The self-relaxation rate coefficients for N_2 ($v = 6$) molecules in the N_2–O_2 and N_2–CO systems were derived from the slope and intercept of the fitted line, yielding values of $(0.73 \pm 0.07) \times 10^{-14}$ cm^3·s^{-1} and $(0.79 \pm 0.11) \times 10^{-14}$ cm^3·s^{-1}, respectively. The collision relaxation rate coefficients for N_2–O_2 and N_2–CO systems were found to be $k_v(O_2) = (6.29 \pm 0.12) \times 10^{-14}$ cm^3·s^{-1} and $k_v(CO) = (11.21 \pm 0.20) \times 10^{-14}$ cm^3·s^{-1}.

In the N_2–O_2 system, the vibrational relaxation rate coefficient associated with collisions between N_2 ($v = 6$) and O_2 molecules is 8.6 times higher than that of N_2–N_2 collisions. In the N_2–CO system, the corresponding relaxation rate coefficient for collisions between N_2 ($v = 6$) and CO molecules is 14.2 times greater than that of N_2–N_2 collisions. Furthermore, the relaxation rate coefficient for the collision of N_2 ($v = 6$) with CO is 1.8 times higher than that of N_2–O_2 collisions and 3.9 times greater than that of homonuclear N_2–N_2 collisions. These results indicate that both O_2 and CO significantly enhance the vibrational relaxation of N_2 ($v = 6$) molecules, with inelastic collisions between N_2 molecules and the buffer gases (O_2 and CO) constituting the predominant mechanism underlying these vibrational relaxation processes. Notably, CO demonstrates the highest quenching efficiency for the vibrational relaxation of N_2 ($v = 6$) among the investigated buffer gases. The relaxation rate coefficient for N_2–CO collisions is approximately 78% higher than that for N_2–O_2 collisions. This difference may be attributed to the isoelectronic nature of N_2 and CO, which possess closely matched vibrational quantum energy levels (N_2: 2358 cm^{-1}, CO: 2169 cm^{-1}). Moreover, the vibrational energy mismatch within the N_2–CO system (189 cm^{-1}) is considerably lower than that within the N_2–O_2 system (778 cm^{-1}), suggesting a more effective vibrational energy transfer mechanism between CO and N_2.

Kurnosov *et al.*[40] computed the state-to-state collisional relaxation rate coefficients for the N_2–CO system at 300 K, reporting values in the range of 10^{-15} cm^3·s^{-1} to 10^{-13} cm^3·s^{-1}. Hong *et al.*[25] used the MQC method to determine the V–V relaxation rate coefficients for N_2–CO, obtaining values between 10^{-16} cm^3·s^{-1} and 10^{-13} cm^3·s^{-1} at the same temperature. Pipe *et al.*[41] experimentally investigated the quenching efficiencies of various molecules on N_2 ($X^1\Sigma_g^+$, $v \geq 5$) and found that O_2 exhibited lower quenching efficiency compared to CO. The results of the present study are in agreement with those reported in the literature.

3.2. Vibrational relaxation mechanisms in the N_2–O_2/N_2–CO systems

The total pressure of the gas mixture in the sample cell was 400 Torr, and the temperature was maintained at 297 K. The excited-state N_2 ($v = 6$) molecules redistribute their energy through inelastic collisions with acceptor molecules, leading to population transfer in vibrational levels with $v < 6$. To further investigate the collisional energy relaxation mechanism of excited-state N_2 ($v = 6$) molecules, we analyze the possible kinetic processes in the system. The near-resonant V–V energy transfer processes that may occur in the N_2–O_2 and N_2–CO systems are as follows:

$$N_2(v=6) + N_2(v=0) \rightarrow N_2(v=5) + N_2(v=1) - 143.24 \text{ cm}^{-1}, \tag{7a}$$

$$N_2(v=6) + N_2(v=0) \rightarrow N_2(v=4) + N_2(v=2) - 229.18 \text{ cm}^{-1}, \tag{7b}$$

$$N_2(v=6) + O_2(v=0) \rightarrow N_2(v=5) + O_2(v=1) + 630.45 \text{ cm}^{-1}, \tag{8a}$$

$$N_2(v=6) + O_2(v=0) \rightarrow N_2(v=4) + O_2(v=3) - 194.80 \text{ cm}^{-1}, \tag{8b}$$

$$N_2(v=6) + CO(v=0) \rightarrow N_2(v=5) + CO(v=1) + 43.45 \text{ cm}^{-1}, \tag{9a}$$

$$N_2(v=6) + CO(v=0) \rightarrow N_2(v=4) + CO(v=2) + 142.11 \text{ cm}^{-1}. \tag{9b}$$

The energy mismatch values on the right-hand side of the above equations were obtained using empirical spectroscopic formulas for diatomic molecules, with the corresponding molecular constants taken from Ref. [42]. The aforementioned kinetic processes primarily involve near-resonant V–V energy transfer between N_2 ($v = 6$) molecules and collisional acceptor molecules (N_2, O_2, or CO). Energetically, energy transfer processes with smaller mismatch values and exothermic characteristics are more likely to occur. In the gas mixture systems, V–RT energy transfer between N_2 ($v = 6$) molecules

and the acceptor molecules may also occur. However, the probability of such processes is generally much lower than that of V–V transfer and can therefore be neglected in most cases.

3.2.1. Single-quantum and multi-quantum relaxation mechanisms in the N_2–O_2 system

At a temperature of 297 K and a total pressure of 400 Torr, time-resolved CARS signals of N_2 molecules at vibrational levels $v = 6$, 5, and 4 were recorded under various O_2 molar ratios (0.3, 0.4, 0.5, 0.6, 0.7, and 0.8). Figure 7 presents the corresponding population evolution curves of N_2 ($v = 6$, 5, 4) under these conditions. As the O_2 molar ratio increases, the dominant relaxation pathway of N_2 ($v = 6$) gradually shifts from single-quantum relaxation to multi-quantum relaxation.

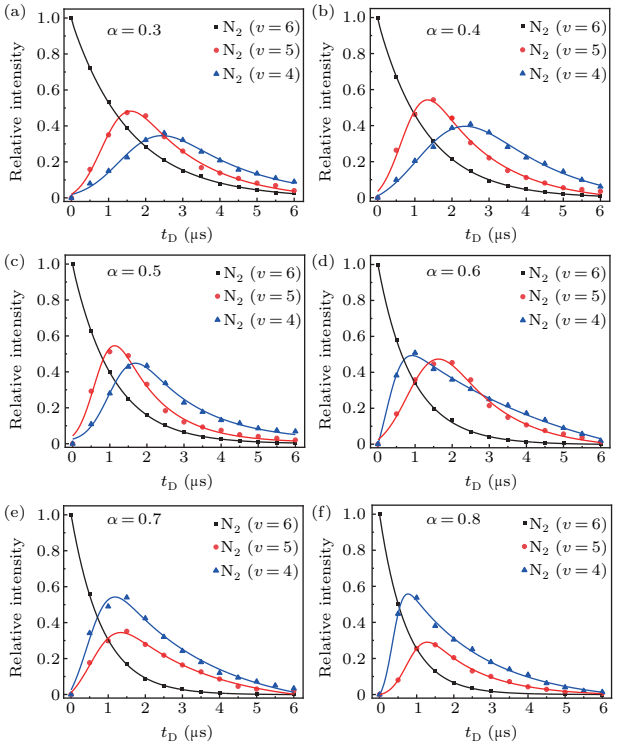


Fig. 7. Population evolution of N_2 at vibrational levels $v = 6$, 5, and 4 under different O_2 molar ratios: (a) $\alpha = 0.3$, (b) $\alpha = 0.4$, (c) $\alpha = 0.5$, (d) $\alpha = 0.6$, (e) $\alpha = 0.7$, (f) $\alpha = 0.8$.

From Figs. 7(a)–7(c), it can be observed that when the O_2 molar ratios are 0.3, 0.4, and 0.5, the population buildup of N_2 molecules at $v = 5$ occurs more rapidly and reaches higher signal intensities. This indicates that the near-resonant single-quantum V–V relaxation between N_2 molecules [corresponding to Eq. (7a)] dominates under these conditions. When the O_2 molar ratios are increased to 0.6, 0.7, and 0.8, as shown in Figs. 7(d)–7(f), the population at $v = 4$ rises significantly faster and reaches higher intensities. This implies that the relaxation of N_2 ($v = 6$) molecules becomes dominated by multi-quantum relaxation pathways, specifically the near-resonant V–V transfer between N_2 and O_2 molecules (as described by Eq. (8b)).

As the O_2 molar ratio increases from 0.3 to 0.5, the population buildup rates at both $v = 5$ and $v = 4$ levels accelerate. Specifically, the peak population time at $v = 5$ decreases from 1.6 μs to 1.2 μs, while that at $v = 4$ shortens from 2.5 μs to 1.8 μs. Under low O_2 concentrations, the collisional energy transfer of N_2 ($v = 6$) is primarily governed by near-resonant single-quantum V–V processes between N_2 molecules. However, with increasing O_2 concentration, the frequencies of near-resonant V–V collisions described by Eqs. (8a) and (8b) increase significantly, accelerating the relaxation of N_2 ($v = 6$). Despite this, single-quantum processes corresponding to Eqs. (7a) and (8a) still dominate under moderate O_2 ratios.

When the O_2 molar ratio reaches 0.6, the multi-quantum near-resonant V–V relaxation process between N_2 and O_2, described by Eq. (8b), becomes significantly enhanced and begins to dominate vibrational energy exchange in the mixture. At this point, the peak population time for N_2 ($v = 4$) is further reduced from 1.8 μs to 0.9 μs. As the O_2 molar ratio continues to increase to 0.7 and 0.8, the multi-quantum collisional relaxation between N_2 and O_2 is further strengthened, leading to even faster population buildup of N_2 ($v = 4$). Under these conditions, the dominant relaxation mechanism of N_2 ($v = 6$) transitions fully to multi-quantum relaxation.

3.2.2. Single-quantum and multi-quantum relaxation mechanisms in the N_2–CO system

At a temperature of 297 K and a total gas pressure of 400 Torr, time-resolved CARS signals of N_2 molecules at vibrational levels $v = 6$, 5, and 4 were measured following degenerate stimulated hyper-raman pumping of N_2 ($v = 6$) under varying CO molar ratios. Figure 8 shows the temporal evolution of population distributions at the $v = 6$, 5, and 4 vibrational levels of N_2 in N_2–CO mixtures with different CO molar ratios. It can be seen that the collisional relaxation pathways of N_2 ($v = 6$) molecules are strongly dependent on the concentration of the acceptor molecule CO. As the CO molar ratio increases, the dominant relaxation mechanism of N_2 ($v = 6$) transitions progressively from multi-quantum relaxation to predominantly single-quantum relaxation.

As shown in Fig. 8(a), when the CO molar ratio is 0.3, the population of N_2 molecules at $v = 4$ increases more rapidly than at $v = 5$, although the peak intensities at both levels are comparable. Under these conditions, N_2 ($v = 6$) molecules primarily undergo vibrational energy exchange via V–V collisions with other N_2 molecules. Due to the small energy mismatches associated with the processes described in Eqs. (7a) and (7b), both transitions occur randomly. Consequently, in the N_2–CO system, rapid multi-quantum V–V relaxation between N_2 molecules dominates vibrational relaxation. At a CO molar ratio of 0.4 (Fig. 8(b)), the populations at $v = 5$ and $v = 4$ reach their peaks simultaneously, with a slightly higher intensity at $v = 5$. This indicates a significant enhancement of the

near-resonant single-quantum V–V relaxation between N_2 and CO, making it the dominant relaxation pathway for N_2 ($v = 6$) molecules. At this concentration, the peak population time at $v = 5$ shortens from 2.5 μs to 1.9 μs, while the peak time at $v = 4$ remains relatively unchanged, indicating suppression of the multi-quantum relaxation channel.

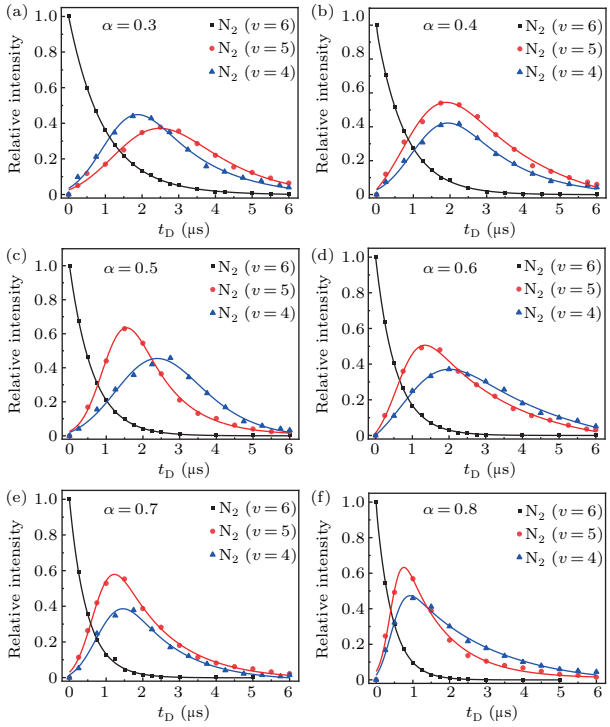


Fig. 8. Temporal evolution of the population distributions of N_2 at vibrational levels $v = 6$, 5, and 4 in N_2–CO mixtures under different CO molar ratios: (a) $\alpha = 0.3$; (b) $\alpha = 0.4$; (c) $\alpha = 0.5$; (d) $\alpha = 0.6$; (e) $\alpha = 0.7$; (f) $\alpha = 0.8$.

When the CO molar ratio increases to 0.5 and 0.6 (Figs. 8(c) and 8(d)), both the population rate and signal intensity at $v = 5$ increase significantly, with the peak time at this level further reduced to 1.4 μs. This confirms that the near-resonant single-quantum V–V relaxation between N_2 and CO (Eq. (9a)) now dominates the vibrational energy transfer process. At higher CO molar ratios of 0.7 and 0.8 (Figs. 8(e) and 8(f)), the population rates at $v = 4$ and $v = 5$ further accelerate, with the corresponding peak times reduced to 0.8 μs and 0.9 μs, respectively. Although the multi-quantum V–V relaxation (Eq. (9b)) becomes more pronounced under these conditions, single-quantum transitions still remain the primary mechanism. This relaxation of vibrationally excited N_2 molecules in the N_2–CO system reflects a dynamic interplay between single- and multi-quantum relaxation modes, where lower energy mismatches energetically favor more efficient energy exchange.

The collisional energy transfer pathways and the corresponding relaxation times of excited-state molecules are closely related to the magnitude of energy gaps. The vibrational energy matching characteristics and near-resonance effects play a pivotal role in the relaxation processes of excited-state molecules. Klatt *et al.*[43] found that near-resonance energy transfer is crucial in promoting V–V exchange during their study of the collisional relaxation rate coefficients of ground-state O_2 ($v = 8$–11) molecules with different collision partners. Mamatimind *et al.*[44] observed near-resonant multi-quantum relaxation processes during the collisional relaxation of vibrationally excited N_2 ($v = 6$) molecules in the N_2–H_2 system. Similarly, Mao *et al.*[45] investigated the rotational relaxation of D_2(1,12) in a D_2–N_2 mixture, revealing that near-resonant multi-quantum relaxation also occurs in the D_2–N_2 system. These near-resonance effects are crucial for understanding energy transfer processes and the collisional relaxation mechanisms.

It is important to note that in mixed gases, the state-to-state V–V energy transfer process between molecular states involves the rapid evolution of excited-state molecular dynamics, typically occurring on the picosecond or sub-picosecond time scale. However, current experimental techniques are still insufficient to accurately resolve the complete energy transfer pathway and its associated rate at such ultrafast timescales. The measurements reported in this study capture the temporal evolution of CARS signals from N_2 molecules across various vibrational energy levels as a function of post-collision delay time. These findings represent statistically averaged data and do not correspond to direct observations of population distributions in specific vibrational states of N_2 molecules.

3.3. Thermal effects on the relaxation mechanisms of N_2 ($v = 6$) molecules

Increased temperature directly affects the translational energy of molecules and collision frequencies, which, in turn, influence the vibrational energy transfer pathways within the system. The results from Figs. 7 and 8 highlight a strong correlation between the concentration of acceptor molecules and the vibrational relaxation mechanisms of excited-state species in the system. In the N_2–O_2 mixture, as the O_2 molar ratio increases, the relaxation mechanism transitions from single-quantum to multi-quantum relaxation. In contrast, in the N_2–CO system, an increase in CO concentration suppresses multi-quantum relaxation, leading to dominance of single-quantum relaxation. Based on these findings, we selectively investigated the temperature dependence of the vibrational relaxation mechanisms of excited-state molecules in mixed systems under both low and high acceptor concentrations. Figure 9 presents the population evolution curves of N_2 molecules in the $v = 5$ and $v = 4$ vibrational levels in the N_2–O_2 system, measured over a temperature range of 297 K–508 K, with O_2 molar ratios of 0.3 and 0.8.

As shown in Fig. 9(a), when the O_2 molar ratio is 0.3, the energy exchange between N_2 ($v = 6$) molecules and the colliding partners is predominantly governed by single-quantum

relaxation. As the temperature increases, the population relaxation rates of N_2 molecules at the $v = 5$ and $v = 4$ vibrational levels accelerate. The population peak time of N_2 ($v = 5$) decreases from 1.6 μs to 0.6 μs, while the peak time for N_2 ($v = 4$) shifts from 2.7 μs to 1.2 μs. This indicates that the increase in temperature enhances molecular thermal motion, significantly elevating the collision frequency between N_2 molecules. Corresponding to Eqs. (7a) and (7b), the near-resonance collision rates for N_2–N_2 also increase with rising temperature.

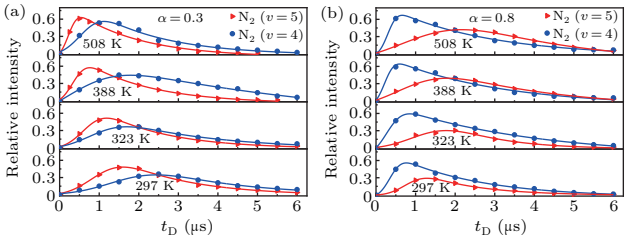


Fig. 9. Evolution of the population distribution of N_2 ($v = 5$, 4) energy levels in the N_2–O_2 system at different temperatures. (a) O_2 molar ratio of 0.3; (b) O_2 molar ratio of 0.8.

As shown in Fig. 9(b), when the O_2 molar ratio is 0.8, the relaxation mechanism of N_2 ($v = 6$) molecules is primarily governed by multi-quantum relaxation via N_2–O_2 collisions. As the temperature increases, the population relaxation rate of N_2 ($v = 4$) remains largely unchanged, but the population intensity increases significantly. In contrast, the relaxation speed of N_2 ($v = 5$) slows down, and its intensity slightly increases. This result suggests that in high O_2 concentration environments, the rise in temperature significantly enhances the collision process between N_2 and O_2 molecules, especially promoting the multi-quantum relaxation process described by Eq. (8b), which is associated with lower energy losses. When the temperature increases from 297 K to 508 K, the population peak time for N_2 ($v = 5$) molecules shifts from 1.4 μs to 2.3 μs. This change is attributed to the competitive effect between the processes described by Eqs. (8a) and (8b), which slows down the energy exchange in single-quantum collisions. Moreover, the increase in temperature enhances the translational energy of the molecules, thereby raising the collision frequency between them. This change increases the likelihood of multiple consecutive collision relaxation processes, further slowing down the population relaxation speed of N_2 molecules at the $v = 5$ level.

Figure 10 shows the population evolution curves of N_2 molecules at different temperatures in the N_2–CO system for the N_2 ($v = 6$, 5, 4) energy levels as a function of delay time. When the CO molar ratio is 0.3, as shown in Fig. 10(a), the increase in temperature accelerates the molecular collision frequency, resulting in enhanced population intensities for the N_2 ($v = 5$, 4) levels and a reduced time to reach peak population. Under these conditions, the single-quantum collision relaxation rate for N_2–N_2 increases significantly with temperature, while the multi-quantum relaxation rate shows minimal variation between 323 K and 508 K. The rise in temperature triggers intense competition between different energy transfer modes in the mixed system, leading to a significant enhancement in the single-quantum relaxation of N_2 ($v = 6$) molecules.

As shown in Fig. 10(b), when the CO molar ratio is 0.8, the relaxation mechanism of N_2 ($v = 6$) molecules transitions from a balance between single-quantum and multi-quantum relaxation to being dominated by single-quantum relaxation as the temperature increases. During this process, the primary relaxation mechanism for N_2 ($v = 6$) molecules is collision relaxation between N_2 and CO molecules. The population dynamics of N_2 molecules at the $v = 5$ and $v = 4$ energy levels slow down with increasing temperature, although the population intensity significantly increases. This indicates that the increase in temperature substantially enhances the single-quantum V–V near-resonance collisions between N_2 and CO. As the temperature rises from 323 K to 508 K, multi-quantum relaxation is notably suppressed. At this point, the population of N_2 molecules at the $v = 4$ level is primarily governed by sequential single-quantum relaxation from $v = 6 \rightarrow v = 5 \rightarrow v = 4$, resulting in a shift in peak population time from 0.9 μs to 2.5 μs. Meanwhile, the enhanced single-quantum V–V near-resonance collisions between N_2 and CO lead to an increase in population peak time at the $v = 5$ level, from 0.7 μs to approximately 1.4 μs.

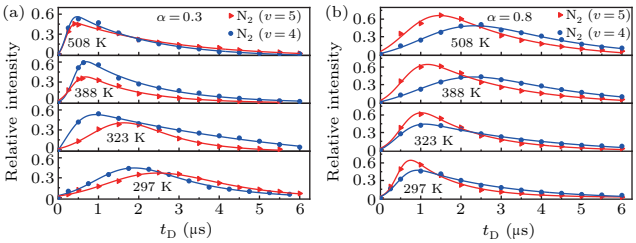


Fig. 10. Population evolution of N_2 ($v = 5$, 4) energy levels in the N_2–CO system at different temperatures. (a) CO molar ratio of 0.3; (b) CO molar ratio of 0.8.

In the system with an O_2 molar ratio of $\alpha = 0.3$, as the temperature increases from 297 K to 573 K, the population peak time for N_2 ($v = 5$) is shortened by approximately 60%, indicating accelerated vibrational relaxation of N_2 ($v = 6$) molecules in accordance with the Arrhenius collision frequency growth law. However, under high O_2 concentrations, the population peak time for N_2 ($v = 4$) is delayed with increasing temperature, suggesting that both single-quantum and multi-quantum relaxation processes are governed by the synergistic effects of inelastic collisions between thermally excited molecules. In the N_2–CO system, the increased temperature enhances the single-quantum V–V process for N_2–N_2 at low CO concentrations and the single-quantum V–V near-resonance interactions between N_2–CO at high CO concentrations. At elevated temperatures, the reduced duration of

molecular collisions weakens the long-range coupling interactions required for multi-quantum processes, while the harmonic vibrational mode of CO facilitates the activation of single-quantum channels in N_2–CO collisions through thermal motion.

4. Conclusion

In this study, the DSHRP technology was utilized to selectively populate N_2 molecules at the $v = 6$ vibrational level in the ground electronic state. The vibrational relaxation behavior of excited N_2 ($v = 6$) molecules was systematically investigated in the N_2–N_2, N_2–O_2, and N_2–CO systems. During the experiment, the total pressure of the gas mixtures was maintained at 400 Torr, and the molar ratios of the acceptor molecules (O_2 and CO) were 0.3, 0.4, 0.5, 0.6, 0.7, and 0.8. The main conclusions drawn from the study are as follows.

(i) At 297 K, the self-relaxation rate coefficients of N_2 ($v = 6$) in the N_2–M systems ($M = N_2$, O_2, CO) were determined to be $(2.85 \pm 0.07) \times 10^{-14}$ cm^3·s^{-1}, $(0.73 \pm 0.07) \times 10^{-14}$ cm^3·s^{-1}, and $(0.79 \pm 0.11) \times 10^{-14}$ cm^3·s^{-1}, respectively. The collisional relaxation rate coefficients between N_2 ($v = 6$) and O_2 or CO were found to be $k_v(O_2) = (6.29 \pm 0.12) \times 10^{-14}$ cm^3·s^{-1} and $k_v(CO) = (11.21 \pm 0.20) \times 10^{-14}$ cm^3·s^{-1}. These results indicate that the vibrational relaxation rate coefficient for the collision of N_2 ($v = 6$) with CO is 3.9 times greater than that for homonuclear N_2–N_2 collisions and 1.8 times higher than that for N_2–O_2 collisions. The presence of O_2 and CO significantly enhances the vibrational relaxation of excited N_2 ($v = 6$), with CO demonstrating a considerably higher efficiency in vibrational energy transfer compared to O_2.

(ii) The vibrational relaxation mechanism of N_2 ($v = 6$) molecules in the N_2–CO and N_2–O_2 systems was systematically elucidated under a total pressure of 400 Torr and a temperature of 297 K. In the N_2–O_2 system, as the O_2 molar ratio increases, the vibrational relaxation mechanism of N_2 ($v = 6$) molecules progressively shifts from being dominated by single-quantum relaxation to being governed by multi-quantum relaxation processes. At a relatively low O_2 molar ratio, the vibrational relaxation of N_2 ($v = 6$) primarily occurs through near-resonant energy transfer via N_2–N_2 collisions, which predominantly result in single-quantum relaxation. Conversely, at a higher O_2 molar ratio, multi-quantum relaxation processes involving smaller energy mismatches in N_2–O_2 collisions become the dominant relaxation pathway. In the N_2–CO system, as the CO molar ratio increases, the vibrational relaxation mechanism of N_2 ($v = 6$) molecules transitions from being predominantly governed by multi-quantum relaxation to being primarily driven by single-quantum relaxation. As the concentration of CO increases, the single-quantum V–V relaxation process with smaller energy defects gradually becomes more prominent in N_2–CO collisions.

(iii) The temperature dependence of N_2 ($v = 6$) molecules relaxation mechanisms in N_2–O_2 and N_2–CO systems was investigated within the temperature range of 297–508 K. The results indicate that as the temperature increases, the enhancement of molecular translational energy and the rising collision frequency significantly influence the vibrational energy transfer process. In gas mixtures, the collisional energy transfer process that dominates the vibrational relaxation of N_2 ($v = 6$) molecules exhibits higher temperature dependence. As the temperature further increases, the near-resonance energy exchange caused by such collisions is significantly enhanced.

Acknowledgment

Project supported by the Natural Science Foundation of Xinjiang Uygur Autonomous Region of China (Grant No. 2024D01C51).

References

[1] Zhang H H, Yu W D, Gao C Z and Qu Y Z 2023 *Chin. Phys. Lett.* **40** 043101
[2] Zhu D H, Zhang B, Shen Y F and Dai K 2011 *Chin. Phys. Lett.* **28** 093401
[3] Zhang W, Shi Y C, Hu B T and Zhang Y 2018 *Chin. Phys. B* **27** 013201
[4] Yang Y, Guo L J, Liu Y, Liu W M, Zhu R Y, Qian S X and Xu C H 2003 *Chin. Phys. Lett.* **20** 589
[5] He C, Horst S M, Riemer S, Sebree J A, Pauley N and Vuitton V 2017 *Astrophys. J. Lett.* **841** L31
[6] Hörst S M and Tolbert M A 2014 *Astrophys. J.* **781** 53
[7] Jasper A W, Pelzer K M, Miller J A, Kamarchik E, Harding L B and Klippenstein S J 2014 *Science* **346** 1212
[8] Fromentin C, Silva T, Dias T C, Morillo-Candas A S, Biondo O, Guaitella O and Guerra V 2023 *Plasma Sources Sci. Technol.* **32** 024001
[9] Hong Q Z, Wang X Y, Hu Y and Sun Q H 2020 *Phys. Fluids* **32** 046102
[10] Pavlov A 2011 *Geomagn. Aeron.* **51** 143
[11] Stüeken E E, Kipp M A, Koehler M C, Schwieterman E W, Johnson B and Buick R 2016 *Astrobiology* **16** 949
[12] Spros sL, Scherf M, Shematovich V I, Bisikalo D V and Lammer H 2021 *Astron. Rep.* **65** 275
[13] Hong Q Z, Wang X Y, Hu Y, Lin X and Sun Q H 2020 *Int. J. Mod. Phys. B* **34** 2040084
[14] Roueff E, Loison J C and Hickson K M 2015 *Astron. Astrophys.* **576** A99
[15] Spezzano S, Caselli P, Sipilä O and Bizzocchi L 2022 *Astron. Astrophys.* **664** L2
[16] Celiberto R, Armenise I, Cacciatore M, Capitelli M, Esposito F, Gamallo P, Janev R K, Laganà A, Laporta V, Laricchiuta A, Lombardi A, Rutigliano M, Sayós R, Tennyson J and Wadehra J M 2016 *Plasma Sources Sci. Technol.* **25** 033004
[17] Huang Y F, Hong Q Z, Gu S D, Wang X Y and Sun Q H 2024 *Phys. Fluids* **36** 106133
[18] Slanger T G, Hwang E S, Bartlett N C M and Kalogerakis K S 2018 *J. Phys. Chem. A* **122** 8114
[19] Gu S D, Hao J A and Wen C Y 2023 *Phys. Fluids* **35** 066116
[20] Chapuisat X, Bergeron G and Launay J M 1977 *Chem. Phys.* **20** 285
[21] Liang J and Donovan E 2024 *Geophys. Res. Lett.* **51** e2024GL110986
[22] Karman T, Koenis M A J, Banerjee A, Parker D H, Gordon I E, van der Avoird A, van der Zande W and Groenenboom G C J 2018 *Nat. Chem.* **10** 549
[23] Guo C M, Zhang H and Cheng X L 2024 *J. Phys. Chem. A* **128** 5435

[24] Garcia E, Lagana A, Pirani F, Bartolomei M, Cacciatore M and Kurnosov A 2016 *J. Phys. Chem. A* **120** 5208

[25] Hong Q Z, Bartolomei M, Coletti C, Lombardi A, Sun Q H and Pirani F 2021 *Molecules* **26** 7152

[26] Hong Q Z, Storchi L, Sun Q H, Bartolomei M, Pirani F and Coletti C 2023 *J. Chem. Theory Comput.* **19** 8557

[27] Yang J W, Hong Q Z, Bartolomei M, Pirani F, Coletti C, Sun Q H and Li J 2025 *Phys. Rev. A* **111** 032804

[28] Andrienko D A and Boyd I D 2018 *J. Thermophys. Heat Transfer* **32** 904

[29] Garcia E, Kurnosov A, Lagana A, Pirani F, Bartolomei M and Cacciatore M 2016 *J. Phys. Chem. B* **120** 1476

[30] Ahn T, Adamovich I V and Lempert W R 2004 *Chem. Phys.* **298** 233

[31] Richards C, Jans E, Gulko I, Orr K and Adamovich I V 2022 *Plasma Sources Sci. Technol.* **31** 034001

[32] Sitz G O and Farrow R L 1994 *J. Chem. Phys.* **101** 4682

[33] Hanisco T F and Kummel A C 1991 *J. Phys. Chem.* **95** 8565

[34] Martínez R Z and Bermejo D 2015 *Phys. Chem. Chem. Phys.* **17** 12661

[35] Xiao Y, Wen L P, Li Z C, Han J, Wu W J, Wang T, Xie Y R and Yang T G 2024 *J. Phys. Chem. Lett.* **15** 11510

[36] Sitz G O and Farrow R L 1990 *J. Chem. Phys.* **93** 7883

[37] Chen M L, Lin W C and Luh W T 1997 *J. Chem. Phys.* **106** 5972

[38] Nie K P, Liu J, Xing J and Alghazi A 2022 *J. Phys. B: At. Mol. Opt. Phys.* **54** 235201

[39] Billing G D and Fisher E 1979 *Chem. Phys.* **43** 395

[40] Kurnosov A K, Napartovich A P, Shnyrev S L and Cacciatore M 2010 *Plasma Sources Sci. Technol.* **19** 045015

[41] Piper L G 1992 *J. Chem. Phys.* **97** 270

[42] Huber K P and Herzberg G 2013 *Molecular Spectra and Molecular Structure: IV. Constants of Diatomic Molecules*, 1st edn. (New York: Springer) pp. 166–498

[43] Klatt M, Ian W M S, Symonds A C, Tuckett R P and Gary N 1996 *J. Chem. Soc., Faraday Trans.* **92** 193

[44] Mamatimin A, Liu J, Habibulla N and Alghazi A 2023 *J. Phys. B: At. Mol. Opt. Phys.* **56** 225201

[45] Mao L, Liu J, Habibulla N and Qiu Y B 2024 *J. Chem. Phys.* **160** 154305